# An experimental demonstration of a new type of proton computed tomography using a novel silicon tracking detector

J. T. Taylor[a),b)]
*Department of Physics, University of Liverpool, Oxford Street, Liverpool L69 7ZE, United Kingdom*

G. Poludniowski[b)]
*Department of Medical Physics, Karolinska University Hospital, SE-171 76 Stockholm, Sweden and Centre for Vision Speech and Signal Processing, Faculty of Engineering and Physical Sciences, University of Surrey, Guildford GU2 7XH, United Kingdom*

T. Price
*School of Physics and Astronomy, University of Birmingham, Birmingham B25 2TT, United Kingdom*

C. Waltham
*Laboratory of Vision Engineering, School of Computer Science, University of Lincoln, Lincoln LN6 7TS, United Kingdom*

P. P. Allport
*School of Physics and Astronomy, University of Birmingham, Birmingham B25 2TT, United Kingdom*

G. L. Casse
*Department of Physics, University of Liverpool, Oxford Street, Liverpool L69 7ZE, United Kingdom*

M. Esposito
*Laboratory of Vision Engineering, School of Computer Science, University of Lincoln, Lincoln LN6 7TS, United Kingdom*

P. M. Evans
*Centre for Vision Speech and Signal Processing, Faculty of Engineering and Physical Sciences, University of Surrey, Guildford GU2 7XH, United Kingdom*

S. Green
*School of Physics and Astronomy, University of Birmingham, Birmingham B25 2TT, United Kingdom*

S. Manger
*Department of Physics, University of Warwick, Coventry CV4 7AL, United Kingdom*

S. Manolopoulos
*University Hospitals Coventry and Warwickshire NHS Trust, Coventry CV2 2DX, United Kingdom*

J. Nieto-Camero
*iThemba LABS, P.O. Box 722, Somerset West 7129, South Africa*

D. J. Parker
*School of Physics and Astronomy, University of Birmingham, Birmingham B25 2TT, United Kingdom*

J. Symons
*iThemba LABS, P.O. Box 722, Somerset West 7129, South Africa*

N. M. Allinson
*Laboratory of Vision Engineering, School of Computer Science, University of Lincoln, Lincoln LN6 7TS, United Kingdom*

(Received 12 July 2016; revised 20 September 2016; accepted for publication 6 October 2016; published 25 October 2016)

**Purpose:** Radiography and tomography using proton beams promise benefit to image guidance and treatment planning for proton therapy. A novel proton tracking detector is described and experimental demonstrations at a therapy facility are reported. A new type of proton CT reconstructing relative "scattering power" rather than "stopping power" is also demonstrated. Notably, this new type of imaging does not require the measurement of the residual energies of the protons.

**Methods:** A large area, silicon microstrip tracker with high spatial and temporal resolution has been developed by the Proton Radiotherapy Verification and Dosimetry Applications consortium and commissioned using beams of protons at iThemba LABS, Medical Radiation Department, South Africa. The tracker comprises twelve planes of silicon developed using technology from high energy physics with each plane having an active area of $\sim 10 \times 10$ cm segmented into 2048 microstrips. The tracker is organized into four separate units each containing three detectors at 60° to one another creating an *x-u-v* coordinate system. Pairs of tracking units are used to reconstruct vertices for protons

  

entering and exiting a phantom containing tissue equivalent inserts. By measuring the position and direction of each proton before and after the phantom, the nonlinear path for each proton through an object can be reconstructed.

**Results:** Experimental results are reported for tracking the path of protons with initial energies of 125 and 191 MeV. A spherical phantom of 75 mm diameter was imaged by positioning it between the entrance and exit detectors of the tracker. Positions and directions of individual protons were used to create angular distributions and 2D fluence maps of the beam. These results were acquired for 36 equally spaced projections spanning 180°, allowing, for the first time, an experimental CT image based upon the relative scattering power of protons to be reconstructed.

**Conclusions:** Successful tracking of protons through a thick target (phantom) has demonstrated that the tracker discussed in this paper can provide the precise directional information needed to perform proton radiography and tomography. When synchronized with a range telescope, this could enable the reconstruction of proton CT images of stopping power. Furthermore, by measuring the deflection of many protons through a phantom, it was demonstrated that it is possible to reconstruct a new kind of CT image (scattering power) based upon this tracking information alone.  [http://dx.doi.org/10.1118/1.4965809]

Key words: proton therapy, particle therapy, silicon strip detector, dosimetry, proton computed tomography

## 1. INTRODUCTION

Although the majority of radiotherapy is still carried out with x-ray beams, a growing number of facilities are now offering charged particle radiotherapy with protons or heavier ions. The advantage of this kind of treatment lies in the dose distribution of charged particles when compared with x-rays. Charged particles (unlike x-rays) deposit the greatest dose toward the end of their range as they come to rest. This region is known as the "Bragg peak" and allows the energy of the charged particle beam to be tuned so concentrating the maximum dose of the beam at a specific location in the body. As such, imaging techniques are critical to ensure that the Bragg peak is located in the tumor and not in the organs and healthy tissue that surround it. An uncertainty on the tumor location or tissue properties at the imaging and treatment planning stage can result in the range of the treatment beam being miscalculated. This may result in an unwanted dose being given to healthy tissue or the tumor not being given the required dose. At present, x-ray CT scans are the usual way to plan a treatment of proton therapy. However, due to the interaction of x-rays and protons with matter being so fundamentally different, the use of an x-ray CT scan to plan a proton therapy treatment results in errors that propagate through the plan into the range of the treatment beam. Ultimately, this affects the amount of healthy tissue that is irradiated during a treatment and could lead to incomplete irradiation of the tumor. It has been proposed that a large portion of this error could be eliminated if it were possible to carry out a number of proton radiographs, or indeed a full proton CT (*p*CT) scan, allowing treatment planning from a *p*CT rather than an x-ray CT. Several experimental efforts are underway to achieve this,[1–4] many of the details of which are summarized and compared here.[5] The method discussed in this paper is not proposed as sufficient by itself for the planning of proton therapy treatment, but rather a complimentary technique to x-ray CT or standard stopping-power *p*CT itself.

A typical *p*CT design is depicted in Fig. 1, although the detector technology used varies widely between prototypes. Such devices contain two detector systems. The first is a set of tracking detectors to provide information on the spatial location of protons as they enter and exit the object to be imaged, and the second is a detector to determine the residual energy or range of the protons after they emerge from the object. In this work, however, we demonstrate a simplified form of tracker-only *p*CT based on scattering, which does not require the use of a range-energy instrument.

The construction of a proton imaging modality is not trivial to achieve. Any system that hopes to provide a high-resolution CT image using protons must be able to correlate multiple measurements of individual protons for a large number of histories in a reasonable time. In particular, for the tracking detector (the focus of this paper), it is necessary that the instrument meet the following requirements:

- High-speed readout: Protons must be individually tracked many millions of times per second with a high efficiency so acquiring an image with a sufficient number of proton histories and a sufficient number of projections in a reasonable time.
- High efficiency: The individual efficiency of the detectors and the overall efficiency for tracking the protons through the system must be high, such that an image is acquired in the shortest possible time with the lowest possible dose to the patient.
- High spatial resolution: The location (and direction) of protons must be known with sub-mm precision in order for the acquired image to have sufficient resolution to be clinically useful.

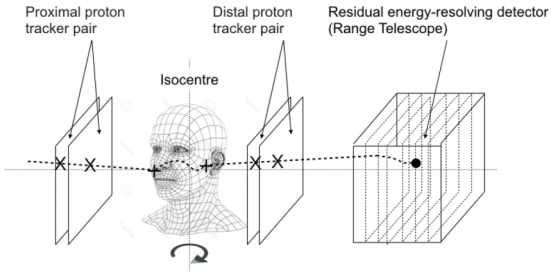


FIG. 1. Conventional *p*CT system concept. Pairs of tracking units labeled here as "proximal" and "distal" describe the trajectory (dashed line) of individual protons through the object to be imaged. A residual energy or range detector placed downstream infers the residual energy of the individual protons after they have been tracked.

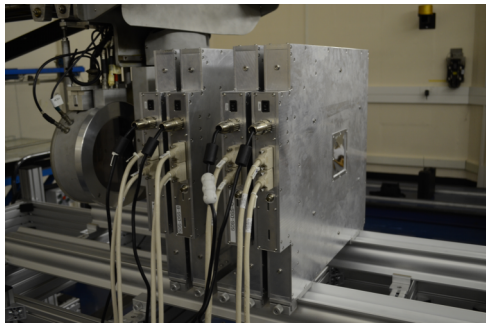

FIG. 2. The PRaVDA silicon tracker setup on an optical bench situated in the proton vault at iThemba LABS. The phantom is situated in the spacing that can be seen between the front and back pair of tracking units.

- Low mass: The tracking detectors themselves should be thin, low mass devices that are relatively transparent to the particles they are trying to measure. This means that the total fractional radiation length ($x/X_0$) of the instrument must be sufficiently low that the spatial resolution of the tracker is not compromised by the multiple-Coulomb scattering (MCS) that the protons undergo whilst traversing it.
- Radiation hard: The detectors and readout electronics are situated directly in the beam and if used for beam monitoring (as well as *p*CT) must deliver the same stable signals over many cycles of treatment and QA. As such, they must be able to withstand the radiation from the treatment beam with its ionizing and nonionizing components.

In this paper, we report on progress made by the Proton Radiotherapy Verification and Dosimetry Applications (PRaVDA) consortium[6] in developing and testing a silicon tracker for *p*CT imaging and dosimetry that meets the above requirements.[5,7–10] The silicon microstrip detectors and readout used were adapted from designs made for the ATLAS experiment based at the High Luminosity Large Hadron Collider (HL-LHC) in CERN, Geneva. Such detector technology has a proven history of providing high efficiency,[11] high precision tracking information at MHz rates, and with excellent radiation hardness characteristics.[12–15]

## 2. MATERIALS AND METHODS

### 2.A. The tracking detector

The tracker comprises twelve detectors separated into four units each containing three detectors. Two units are placed on either side of the phantom to be imaged as shown in Fig. 2. Each tracking unit has its three detectors held at an angle of 60° with respect to one another in an *x*-*u*-*v* coordinate system which allows the measurement of multiple particles simultaneously whilst minimizing ambiguities in the reconstructed hits and tracks. Assembly, construction, and readout of the tracking units are discussed in more detail here.[16] Each silicon microstrip detector has a nominal thickness of 150 $\mu$m and is made from *n*-in-*p* silicon segmented into 2048 strips, with 1024 readout on each side of the detector. Each strip has a pitch of 90.8 $\mu$m and a length of 4.8 cm and is wire-bonded to a custom built application-specific integrated circuit (ASIC) for readout. The ASIC is designated rapid high-speed extended ASIC (RHEA) and the chip is a binary device outputting a strip address when a signal is detected over a certain threshold. There are two tunable thresholds in order to allow the presence of a double hit on each of the strips, the likelihood of which increases for high fluence. If multiple events are detected during a single readout cycle with small spatial separation, the probability of charge being deposited on the same strip increases. In this case, the presence of a hit above both thresholds can be used along with the spatial information from the strip address to disentangle the events in the tracking routine. Further details on the layout and electrical characteristics of the sensor and RHEA chip are reported here.[17] The sensitive area of the detectors was constrained by the available space on a standard 6-in. silicon wafer and when arranged in the proposed *x*-*u*-*v* configuration provides an imaging area of ~9 cm diameter.

To produce the tracks of protons passing through the phantom, data recorded from each ASIC comprise both a strip address and a time stamp. These data are sampled by the RHEA chip at a rate of 104 MHz.

This allows a maximum of four channels to be readout from each ASIC. This gives the possibility to detect up to four separate protons per ASIC per readout cycle when the system is triggered using a signal from the (iThemba) separated sector cyclotron RF with its beam spill repetition rate of 26 MHz. By correlating the position (strip address) and time (stamps) of events across planes, proton "hits" are reconstructed in each tracker unit by forming an effective pixel using the crossing of the strips from two or three of the planes. The vector joining two of these pixels in separate units describes the trajectory of the proton as it enters and exits the phantom. The use of three silicon planes for each coordinate measurement allows the possibility to cope with high fluence since there is an additional piece of positional information available and an angle between the planes of <90° which reduces the number of ambiguous hit locations when multiple particles are present.[11] It also supplies an element of redundancy to the reconstruction such that events that pass through dead or noisy

channels on a layer can still be reconstructed (or corrected) provided reliable information can be extracted from the other two layers in the tracking unit. This allows for a higher overall tracking efficiency than that available for a tracker comprised of only eight planes orientated only in orthogonal pairs for obtaining $x$ and $y$ positions (the typical configuration in $p$CT prototypes).

### 2.B. Experimental facilities and acquisition

The tracker and phantom were irradiated in the "proton vault" at iThemba LABS, South Africa where beams of protons are available up to a nominal energy of 191 MeV (240 mm range in water). The beams are produced by a cyclotron and are made available for both experimental work and proton therapy with a diameter up to 10 cm. In order to produce a beam of this size with the required symmetry and uniformity, a number of different scattering and collimation components are used upstream of the final nozzle in the vault. In order to produce the lower energy beams typically needed for proton therapy (and made use of in this work), a pair of graphite wedges can be inserted into the path of the beam degrading the energy down to a minimum range of 30 mm in water (~55 MeV). These degraders are situated before the proton vault which contains a large area transmission ionization chamber used to monitor the fluence. The range of currents available from the cyclotron can be varied such that the proton current available in the vault is in the range from 0.1 to 100 nA. In order for the cyclotron to provide stable lower currents, i.e., <1 nA used in this work, filters applied after the ion source can reduce stable higher currents by a factor of $10^{-2}$ or $10^{-4}$.

For the work presented here, beams with proton kinetic energies of either 191 or 125 MeV were selected. The 191 MeV selection was used for setup, alignment, and calibration of the tracker, and the experimental data for the CT scan were taken with the 125 MeV beam. We note that an incident energy of 125 MeV (118 mm in water) is lower than would be necessary for clinical imaging of most body sites on most subjects. However, the value was appropriate for the object imaged, the size of which was limited by the area of the prototype tracking detectors. A collimated beam of 85 mm diameter and a low proton current of $\sim 10^5$ cm$^{-2}$ s$^{-1}$ were used in order for data acquisition and tracking to be as straightforward as possible. Data were acquired for a total of 6 s per projection in order to acquire enough events to fill the available local memory attached to the readout of each layer. A total of 36 equally spaced angular projections were acquired spanning 180°, with between 15 and $50\times10^6$ events reconstructed per projection.

The object imaged in this experiment was a spherical phantom of poly(methyl methacrylate) (PMMA) with a diameter of 75 mm. This was suspended in between the second and third tracking units (see Fig. 2) on a rotary stage. Situated inside the phantom were several cylindrical inserts of materials, three of which were high contrast with respect to PMMA (lung and cortical bone tissue substitutes and an air cavity).[18]

### 2.C. Scattering power and *p*CT reconstruction

Scattering power, $t_i$, of a material, $i$, is defined as the rate-of-change of mean-square scattering-angle with depth, such that

$$t_i = \frac{d\bar{\vartheta}^2}{dz}, \tag{1}$$

where $\vartheta$ is the total angular deflection at a depth $z$ in a material and the bar denotes the mean for a large ensemble of particles. The mechanism underlying the increase in deflection with depth is MCS. The relative scattering power can be defined as

$$\rho_i = \frac{t_i}{t_w}, \tag{2}$$

where $t_w$ is the scattering power for water.

In this work, CT reconstruction was implemented to reconstruct relative scattering power. The total deflection-angle squared was determined for each proton based on the measurements of spatial position in each of the four tracker units. The total mean-square angular deflection can be approximated as

$$\vartheta^2 = (\Omega_{x,\text{in}} - \Omega_{x,\text{out}})^2 + (\Omega_{y,\text{in}} - \Omega_{y,\text{out}})^2, \tag{3}$$

where $\Omega_x$ and $\Omega_y$ refer to the direction cosines of the proton in $x$ and $y$ directions, respectively, orthogonal to the beam direction. The subscripts in and out refer to the proton direction determined from the first and second pairs of detectors, respectively. A small-angle approximation has been assumed, i.e., $\sin\vartheta \approx \vartheta$.

The reconstruction method was a modified implementation of a backprojection-then-filtration algorithm presented elsewhere.[19] In that work, the water-equivalent path-length (WEPL) for each proton (in terms of energy loss) was backprojected along a cubic-spline estimate of its nonlinear path in the subject. This allowed reconstruction of a 3D image of relative stopping power. Here, instead, the squared deflection angle for each proton was backprojected, producing a voxel-dependent estimate of mean-square angle in each projection. Prior to the summation of contributions from all projections, the mean-square angle in each voxel was converted to water-equivalent path-length (in terms of scattering) using a relationship derived from Monte Carlo simulations.

Monte Carlo calculations were performed for 125 MeV protons incident on water slabs of thicknesses ranging from 2 to 110 mm, using the FLUKA code.[20] From these simulations, the relationship between mean-square scattering-angle and water-equivalent path-length was determined. Successive 3-sigma and then 2-sigma cuts on positional and angular deflection were applied to the exiting protons, to suppress contributions from the single-scattering tails of MCS and from inelastic nuclear interactions. The same cuts were applied to the projection images of the test phantom.

CT reconstruction was performed using $15\times10^6$ protons per projection (a total of $540\times10^6$ protons over 36 projections) with a voxel size of 1 mm$^3$. Postprocessing with a 3D Gaussian filter of width 0.7 mm was applied to suppress noise.

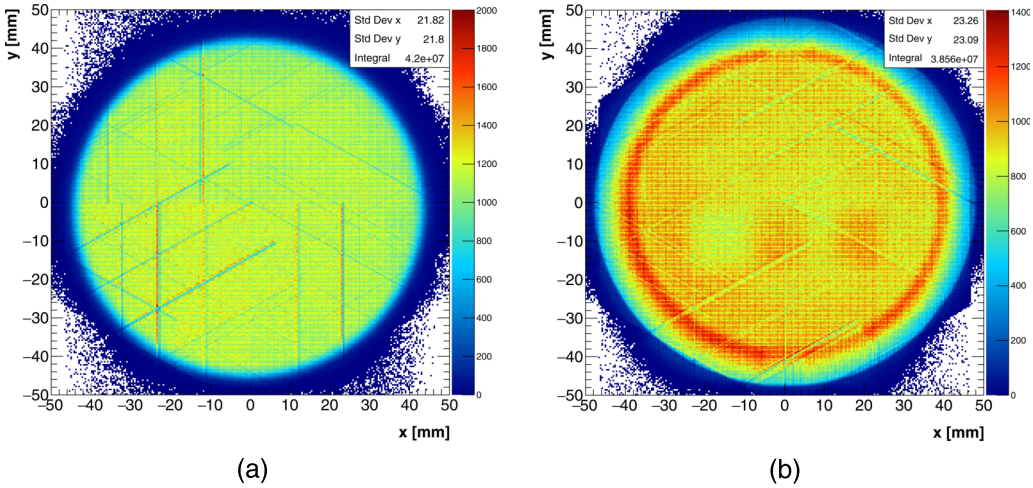


FIG. 3. Radiographs based upon measured fluence shown with bins of 400 $\mu$m for the degraded 125 MeV proton beam passing through an 85 mm diameter collimator. Measurements are shown for the first tracking unit (a), situated closest to the collimator, and the fourth tracking unit (b) situated furthest from the collimator and after the phantom. Dispersion of the beam and the edge of the spherical phantom are clearly visible in (b) along with the appearance of three high contrast inserts. The beam is traveling along the $z$-axis.

## 3. RESULTS

For the chosen $p$ CT energy of 125 MeV, the probability of tracking a proton between pairs of successive layers was found to have a mean value of >93%, and the total proportion of events tracked through the complete system with the phantom in place was found to be >80% when normalized to the mean events per layer seen in the first tracking unit.

The data describing the reconstructed hits in each of the tracking units can be represented as a fluence map, examples of which are shown in Fig. 3. Areas of lower efficiency are visible where only two planes can be used for reconstruction due to dead or noisy strips that were turned off in the DAQ or subsequent analysis. These channels represent 1% of the total channels in the tracker, a level that was deemed satisfactory for a prototype device. In future measurements, improved calibration for noisy channels could reduce this proportion further and in a fully commercial system selection criteria for detectors and ASICs could be applied such that each tracking layer had no defective channels present.

In addition to enabling the determination of fluence maps, the positional information from each tracking unit can be used to give a measurement of the properties of the proton beam, such as the lateral angles $\vartheta_x$ and $\vartheta_y$ in the planes orthogonal to the beam direction. These are shown for 125 and 191 MeV protons passing through the tracker without the phantom, as well as for 125 MeV protons with the phantom in place in Fig. 4. The asymmetry between $\vartheta_x$ and $\vartheta_y$ and the small difference in FWHM are attributed to imperfect alignment of the tracker planes to each other resulting in a slight bias in the resolution of $y$ over $x$. The change in the angular distributions for the degraded 125 MeV proton beam is relatively small when compared with the full energy 191 MeV beam due to the degraders being several meters

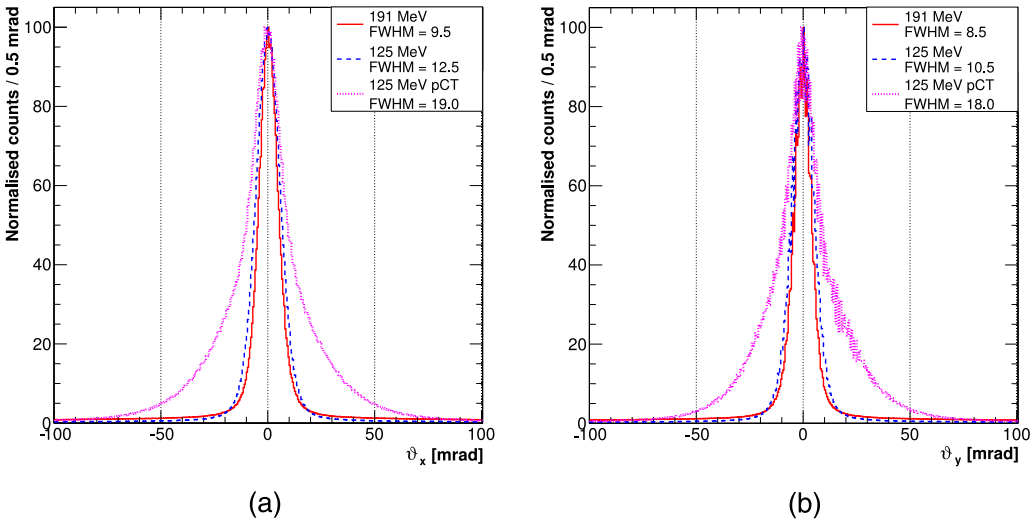


FIG. 4. Deflection angles of protons into the $x$ (a) and $y$ (b) planes which are the axes orthogonal to the direction of motion of the beam. These angles are measured by subtracting the "incoming" angle measured with the first pair of tracking units from the "outgoing" angle measured second pair of tracking units. Distributions are shown for the full energy beam, the degraded 125 beam and the 125 MeV beam with the phantom in place, each with an 85 mm collimator.

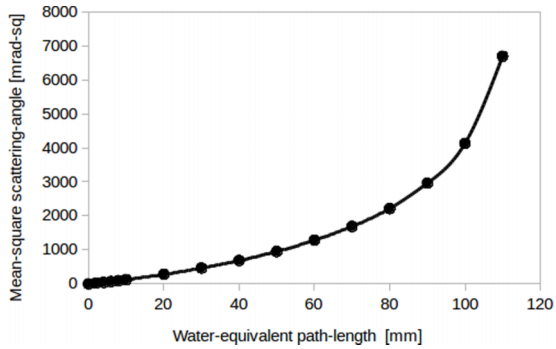


FIG. 5. Relationship between water-equivalent path-length and mean-square scattering angle, as derived from Monte Carlo simulations.

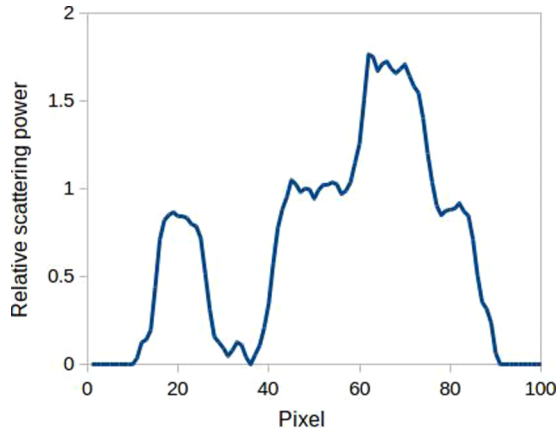


FIG. 7. Line-profile of relative scattering-power. The data correspond to the horizontal row indicated by a pair of lines in Fig. 6.

from the isocenter (phantom/patient location) before which the beam is collimated several times removing any protons that have undergone large angle scattering.

The scattering power *p*CT reconstruction was created by combining the positional information from the four tracking units. The Monte Carlo-derived relationship between WEPL and mean-square scattering angle is presented in Fig. 5. A reconstructed slice through the phantom is presented in Fig. 6 along with a conventional x-ray image of the same slice location. The tissue-substitute materials are clearly visible. The imaging dose for the *p*CT scan was estimated as 1.3 cGy at the center of the phantom (assuming a tracking efficiency of 80% for incident protons). In Fig. 7 a line profile is shown corresponding to the horizontal line in Fig. 6. Note that the background material (PMMA) is expected to have a relative scattering power close to one, as the lower effective atomic number compared to water is compensated for by a higher density.[21]

## 4. DISCUSSION

The results from the tracking detector system demonstrated a high efficiency for track reconstruction (>80%). This is noteworthy as the implication of a low efficiency would be a higher imaging dose for a patient. Note that a proportion of event losses was due to proton inelastic interactions in the phantom and not entirely due to limitations in detection efficiency.

The first important element of novelty in this work is a unique proton tracking detector system in the context of proton therapy that utilizes radiation hard silicon strip detectors in a nonorthogonal configuration. This has been demonstrated to provide a high track-reconstruction efficiency but will also enable operation at high fluence rates for treatment beam monitoring.

A second important innovation was the reconstruction of the first experimental images for proton scattering CT. Given the low number of projections used for reconstruction and the prototype nature of the detector system, the image quality is very encouraging. This modality requires only a tracking system (no energy or range detector). Relative scattering-power images may be useful in several ways, such as imaging guidance with a simplified *p*CT system and in providing

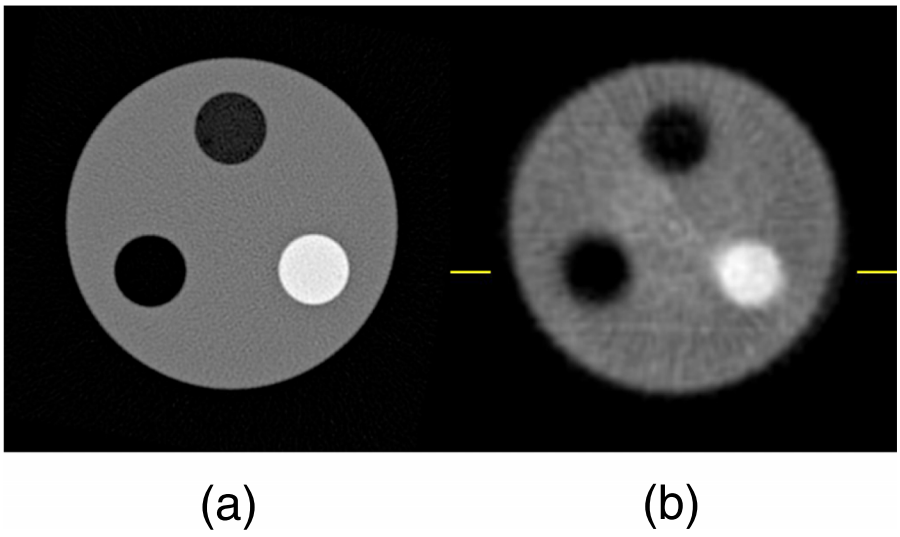


FIG. 6. Slice images of the PRaVDA tissue-substitute phantom using: (a) x-ray CT and (b) proton scattering-power CT. The insert materials present are lung substitute (top), cortical bone substitute (bottom right), and air (bottom left).

valuable information for dose calculations (scattering-power in the patient determines the lateral spread of the treatment beam with depth). In future studies, experimental calibration of the system using a set of plastic slabs is planned. This will enable an improved relationship between water-equivalent path-length and mean-square scattering angle to be derived, without resort to the modeling assumptions inherent in Monte Carlo calculation.

It is appropriate to note that imaging using the angular deflection of protons has been proposed before and planar images of median scattering-angle have been demonstrated experimentally.[22] Tomographic reconstructions of inverse scattering length (closely related to absolute scattering-power) have been demonstrated in simulation.[23,24] Further, we note that nuclear scattering tomography (NST) with protons has long been established, but this relies on very different principles (wide-angle single scattering).[25]

In addition to demonstrating the first experimental CT images using multiple scattering, there are two noteworthy additional features of this work. First, the backprojection-filtering approach proposed is a high-resolution algorithm for proton scattering tomography accommodating nonlinear proton paths. Second, the approach of reconstructing of *relative* scattering-power rather than absolute scattering-power has clear advantages, as the latter quantity is nonlocal and a more problematic quantity.[21] We note that a high-resolution tracker-only *p*CT algorithm has recently been proposed,[26] but this was using an entirely different mechanism for contrast: attenuation due to inelastic nuclear interactions.

Future work will report on the addition of a "range-telescope" to infer each proton's exit energy (as illustrated in Fig. 1). This will permit reconstruction of relative stopping power in addition to relative scattering-power. The complete PRaVDA system will provide a prototype of the first fully solid state *p*CT scanner constructed using silicon detectors for both the tracking and residual-range measurements of protons.

We note that in order to image larger, more clinically relevant areas using the scattering power technique, higher energy beams of protons would be required. This would ensure both that the protons can pass through the object with adequate momentum to be measured and also that they have undergone a sufficiently low amount of MCS such that the information on their trajectory can still be reliably extracted. Simulations by our group have suggested that scattering-power *p*CT has comparable spatial resolution to stopping-power *p*CT with patient-sized objects, albeit with substantially higher noise. A detailed comparison of the techniques, however, is beyond the scope of this work.

## 5. CONCLUSION

Beams of protons with nominal energies of 125 and 191 MeV were successfully tracked through a phantom containing inserts of different tissue equivalent material. This was carried out using a novel tracker system of silicon microstrip detectors. During the *p*CT scan, a high track-reconstruction efficiency was demonstrated (>80%) and using the tracking system, a new type of tracker-only *p*CT was demonstrated for the first time. In this new modality, the contrast can be attributed to the scattering power of the materials through which the protons pass.

## ACKNOWLEDGMENTS

The authors would like to thank the members of the PRaVDA consortium, aSpect Systems GmbH, and ISDI, Ltd., for their contributions and discussion of the results presented in this paper, and Micron Semiconductor, Ltd., for production of the silicon strip detectors. The authors would also like to thank the operators and physicists at iThemba LABS, South Africa for producing and maintaining the proton beams that were used to make the measurements presented here. This work was supported by a Wellcome Trust Translation Award (Grant No. 098285).

## CONFLICT OF INTEREST DISCLOSURE

The authors have no COI to report.

[a]Author to whom correspondence should be addressed. Electronic mail: jtaylor@hep.ph.liv.ac.uk

[b]J. T. Taylor and G. Poludniowski contributed equally to this work.

[1]U. Amaldi, A. Bianchi, Y. Chang, A. Go, W. Hajdas, N. Malakhov, J. Samarati, F. Sauli, and D. Watts, "Construction, test and operation of a proton range radiography system," Nucl. Instrum. Methods Phys. Res., Sect. A **629**, 337–344 (2011).

[2]M. Scaringella *et al.*, "The PRIMA (PRoton IMAging) collaboration: Development of a proton computed tomography apparatus," Nucl. Instrum. Methods Phys. Res., Sect. A **730**, 178–183 (2013).

[3]R. P. Johnson *et al.*, "A fast experimental scanner for proton CT: Technical performance and first experience with phantom scans," IEEE Trans. Nucl. Sci. **63**, 52–60 (2016).

[4]V. A. Bashkirov, R. P. Johnson, H. F.-W. Sadrozinski, and R. W. Schulte, "Development of proton computed tomography detectors for applications in hadron therapy," Nucl. Instrum. Methods Phys. Res., Sect. A **809**, 120–129 (2016).

[5]G. Poludniowski, N. Allinson, and P. Evans, "Proton radiography and tomography with application to proton therapy," Br. J. Radiol. **88**, 20150134 (2015).

[6]The PRaVDA consortium (accessed 2016).

[7]G. Poludniowski, N. Allinson, T. Anaxagoras, M. Esposito, S. Green, S. Manolopoulos, J. Nieto-Camero, D. Parker, T. Price, and P. Evans, "Proton-counting radiography for proton therapy: A proof of principle using CMOS APS technology," Phys. Med. Biol. **59**, 2569–2581 (2014).

[8]M. Esposito *et al.*, "CMOS active pixel sensors as energy-range detectors for proton computed tomography," J. Instrum. **10**, C06001 (2015).

[9]T. Price *et al.*, "Expected proton signal sizes in the PRaVDA range telescope for proton computed tomography," J. Instrum. **10**, P05013 (2015).

[10]T. Price and PRaVDA Consortium, "PRaVDA: High energy physics towards proton computed tomography," Nucl. Instrum. Methods Phys. Res., Sect. A **824**, 226–227 (2016).

[11]H. Spieler, *Semiconductor Detector Systems* (Oxford University Press, Oxford, U.K., 2005), Vol. 12.

[12]ATLAS Collaboration, "Letter of intent for the phase-II upgrade of the ATLAS experiment," Technical Report CERN-LHCC-2012-022 ; LHCC-I-023, 2012.

[13]P. P. Allport, G. Casse, M. Lozano, P. Sutcliffe, J. Velthuis, and J. Vossebeld, "Performance of p-type micro-strip detectors after irradiation to $7.5\times10^{15}$ p/cm$^2$," in *2004 IEEE Nuclear Science Symposium Conference Record* (IEEE, 2004), Vol. 2, pp. 1170–1173.

[14]G. Casse *et al.*, "First results on charge collection efficiency of heavily irradiated microstrip sensors fabricated on oxygenated p-type

silicon," Nucl. Instrum. Methods Phys. Res., Sect. A **518**, 340–342 (2004).
[15]G. Casse, P. Allport, S. M. i Garcia, M. Lozano, and P. Turner, "Performances of miniature microstrip detectors made on oxygen enriched p-type substrates after very high proton irradiation," Nucl. Instrum. Methods Phys. Res., Sect. A **535**, 362–365 (2004).
[16]J. T. Taylor, C. Waltham, T. Price, N. M. Allinson, P. P. Allport, G. L. Casse, A. Kacperek, S. Manger, N. A. Smith, and I. Tsurin, "A new silicon tracker for proton imaging and dosimetry," Nucl. Instrum. Methods Phys. Res., Sect. A **831**, 362–366 (2016).
[17]J. T. Taylor, P. P. Allport, G. L. Casse, N. A. Smith, I. Tsurin, N. M. Allinson, M. Esposito, A. Kacperek, J. Nieto-Camero, T. Price, and C. Waltham, "Proton tracking for medical imaging and dosimetry," J. Instrum. **10**, C02015 (2015).
[18]These materials were samples of the so-called 'Barts materials' and were supplied by Leeds Test Objects (Leeds, UK). Composition codes were: LN10 (lung) and SB5 (cortical bone).
[19]G. Poludniowski, N. Allinson, and P. Evans, "Proton computed tomography reconstruction using a backprojection-then-filtering approach," Phys. Med. Biol. **59**, 7905–7918 (2014).
[20]A. Ferrari, P. R. Sala, A. Fasso, and J. Ranft, "FLUKA: A multi-particle transport code (program version 2005)," Technical Report CERN–2005–010, 2005.
[21]B. Gottschalk, "On the scattering power of radiotherapy protons," Med. Phys. **37**(1):352–367 (2010).
[22]T. Plautz *et al.*, "200 mev proton radiography studies with a hand phantom using a prototype proton CT scanner," IEEE Trans. Med. Imaging **33**, 875–881 (2014).
[23]C. Bopp, J. Colin, D. Cussol, C. Finck, M. Labalme, M. Rousseau, and D. Brasse, "Proton computed tomography from multiple physics processes," Phys. Med. Biol. **58**, 7261–7276 (2013).
[24]C. Bopp, R. Rescigno, M. Rousseau, and D. Brasse, "Quantitative proton imaging from multiple physics processes: A proof of concept," Phys. Med. Biol **60**, 5325–5341 (2015).
[25]R. W. Schulte and V. A. Bashkirov, "Proton scattering analysis system," U.S. patent 8,632,448 (January 21, 2014).
[26]C. Quiñones, J. Létang, and S. Rit, "Filtered back-projection reconstruction for attenuation proton CT along most likely paths," Phys. Med. Biol. **61**, 3258–3278 (2016).